

Article

Effect of Train Vibrations on the Dynamic Response of a Multi-Span Double-Curved Brick Arch Thin-Shell Factory of Changleyuan

Yefeng Liu ^{1,*}, Jianhui Si ¹ , Yuan Zhou ¹, Peiyuan Ma ¹, Yi Wang ¹, Ming Zhou ², Junpeng Ju ² and Xiaoyu Niu ²

¹ School of Civil Engineering and Architecture, Xi'an University of Technology, Xi'an 710048, China; sjhfr@xaut.edu.cn (J.S.); zhoyuan980729@163.com (Y.Z.); 13679128258@163.com (P.M.); 18829361654@163.com (Y.W.)

² Shaanxi Ancient Construction Garden Construction Group Co., Ltd., Xi'an 710048, China; zmzjt1999@163.com (M.Z.); jujunpeng@163.com (J.J.); 18161958966@163.com (X.N.)

* Correspondence: 13465856157@163.com

Abstract: The dynamic characteristics of a multi-span double-curved brick arch thin-shell factory of Changleyuan in Baoji City and the dynamic response to train vibration load were studied using field dynamic tests and finite-element numerical simulations, and a vibration evaluation of the thin-shell factory was carried out. The results showed that the first-order frequency of the thin-shell factory was 6.24 Hz in the horizontal direction (east–west) and 9.31 Hz in the vertical direction. Moreover, it was established that the horizontal vibration is the overall vibration of the factory, while the vertical vibration is the individual vibration of the double-curved brick arch. In addition, the self-oscillation frequency obtained from the numerical simulation results was greater compared with the field measurements, with a maximum error rate of 7.14%. Both in acceleration and velocity, the vertical vibration for each measurement point was larger than the horizontal vibration, and the farther away from the railroad, the smaller the vibration. The vibration of the velocity at the bottom of the arch was almost the same as that at the top of the arch, while the acceleration vibration at the bottom of the arch was significantly larger than that at the top of the arch, with an average amplitude of 40.64%. For every 20 km/h increase in train running speed, the average increase in vertical acceleration amplitude, vertical velocity amplitude, horizontal acceleration amplitude, and horizontal velocity amplitude for each measurement point of the thin-shell factory was 35.4%, 29.8%, 23.7%, and 12.5%, respectively. When $v = 150$ km/h, the maximum velocity amplitude for each measurement point of the thin-shell factory was 1.163 mm/s, which is less than the security specification limit of 2.5 mm/s, such that the security of the thin-shell factory meets the requirement, and the maximum horizontal velocity amplitude was 0.272 mm/s, which is close to the integrity specification limit of 0.27 mm/s, such that the integrity of the thin-shell factory just exceeds the requirement; so it is suggested that train running speeds should not exceed 150 km/h and that the thin-shell factory needs to strengthen the monitoring and protection of its integrity.

Keywords: thin-shell factory; dynamic characteristic; train vibration load; dynamic response; vibration evaluation



Citation: Liu, Y.; Si, J.; Zhou, Y.; Ma, P.; Wang, Y.; Zhou, M.; Ju, J.; Niu, X. Effect of Train Vibrations on the Dynamic Response of a Multi-Span Double-Curved Brick Arch Thin-Shell Factory of Changleyuan. *Buildings* **2023**, *13*, 2400. <https://doi.org/10.3390/buildings13092400>

Academic Editor: Cinzia Buratti

Received: 5 September 2023

Revised: 18 September 2023

Accepted: 20 September 2023

Published: 21 September 2023



Copyright: © 2023 by the authors. Licensee MDPI, Basel, Switzerland. This article is an open access article distributed under the terms and conditions of the Creative Commons Attribution (CC BY) license (<https://creativecommons.org/licenses/by/4.0/>).

1. Introduction

With the rapid development of China's economy and urbanization in recent years, a transportation system compatible with modern cities has also developed in an all-round, multi-level, and three-dimensional manner; in particular, railroads have expanded, being favored by customers because they offer large capacity, high speed, punctuality, convenience, and comfort [1]. Transportation systems have played an important role in promoting the economic development of urban areas and facilitating urban travel; however, the consequent traffic vibration problem has become a growing concern.

Xia et al. [2] studied the vibration response of the Beijing Liao dynasty Liangxiang Tower in the horizontal direction under different train excitations through field tests and numerical simulations and found that the vibration velocity response of the Liangxiang Tower under the action of freight trains was greater than that of passenger trains. Qiao et al. [3] carried out field tests and a theoretical analysis of the vibration elevation response mechanism of the ancient city wall of Jingzibao based on various working conditions and showed that the vibration velocity at the top of the wall was larger than that at the bottom. Further, the vibration amplification effect was mainly influenced by vehicle load and driving speed. Zhang et al. [4] studied the dynamic characteristics of the Xi'an Drum Tower and its dynamic response under different operation modes of Metro Line 6, assessing its vibration performance according to the relevant national codes. Tian et al. [5] found that the vibration acceleration amplitude of high-speed railroad tunnel lining arches increased with an increase in vehicle speed, and the lateral and vertical vibrations of the arches showed different transmission laws. Mykola Karpenko et al. [6] conducted theoretical and experimental research on a composite pneumatic tire used in transport engineering, and the obtained results indicate that the offered methodology can be used in numerical simulations for composite tire investigations and considering material viscoelastic properties. Masoud et al. [7] comparatively studied the vibration characteristics of ground and subway trains by examining the vibrations of buildings at six locations in the Boston area. Hinzen [8] analyzed the dynamic response of Cologne Cathedral under vibratory loads from subway trains through field measurements, evaluated the safety of the structure, and proposed vibration-damping measures. Javad et al. [9] established a finite-element model of the track and surrounding buildings to predict the safe distance between the subway line and the buildings and verified the model's validity and practicality. Agostinacchio et al. [10] studied the vibration response induced by heavy vehicles under different road surfaces and found that vehicle dead weight, traffic volume, and road surface unevenness are the factors that influence vibration transmission. Ju et al. [11] studied and compared the dynamic response of finite-element analysis and field measurements and established a finite-element model that can be used to simulate soil vibrations caused by high-speed trains traveling over bridges.

The vibrations generated by train operations can cause a dynamic response in surrounding buildings and have a serious impact on the safety of buildings [12]. Old industrial buildings are the birthplace of modern industry and have high historical, scientific, and social value. Therefore, it is important to conduct research on the influence of train vibrations on old industrial buildings. This study considered the thin-shell factory of Changleyuan in Baoji City as the research object and analyzed its dynamic characteristics via a field dynamic test and a finite-element numerical simulation; further, the dynamic response of the factory under the action of train vibration load was studied, and a vibration evaluation of the factory was carried out.

2. Project Overview

The thin-shell factory is the most well-preserved anti-war industrial site in China. It is famous at home and abroad and known as "one of the greatest miracles of China during the war" [13]. The thin-shell factory was the first industrial production line supporting the war in the northwest, and it is also a testament to the patriotism of industry entrepreneurs. It has been a witness to the "industrial cooperation" movement and the birthplace of modern industry in Baoji. Its protection and utilization provide a good example of the preservation of modern industrial heritage and support the economic development of the surrounding area.

The thin-shell factory is located in the flat area at the foot of Changleyuan; the structure is situated just over 30 m away from the Longhai Railway (Figure 1). The three groups of buildings constitute six factories in total, each with a depth of 15 m, a width of 20 m, and a surface area of 300 m². The thin-shell factory as a whole faces south; each factory has four doors, and every two factories are connected by a door in the middle (Figure 2).

The factories have similar structural features, such as the brick masonry walls; the height of the east and west side walls (6 m), each of which have four brick columns; and the highest point of the north and south walls (8.5 m), each of which have two brick columns. In addition, the top of the factory exhibits a two-way arch structure; the span of the main arch is 14.5 m, with a vector height of 2.6 m, and the span of the secondary arch is 2 m, with a vector height of 0.55 m. Each factory has 10 groups of these arches, which are connected in the direction of the secondary arch to form the overall large-span roof. The arch structure is made of square bricks, forming a unique thin-shell structure. This approach enabled the construction of large-span structures in times when there were extreme shortages of materials and which could not have been achieved by utilizing wood. This type of large-span factory provided excellent conditions for industrial development. A two-way arch thin-shell structure of this sort is relatively rare in China, and it has an important role in the study of the development of the construction industry at that time. An image of the arch structure is shown in Figure 3.



Figure 1. A map showing the location of the thin-shell factory of Changleyuan, Baoji City.



Figure 2. An image showing the outer appearance of the thin-shell factory.

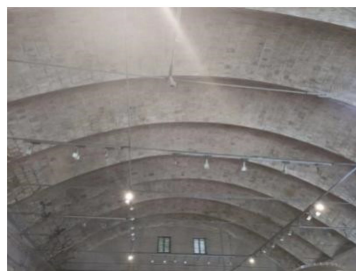


Figure 3. An image showing the arch structure in detail.

3. Field Dynamic Test

Donghua's 32-channel DH5983 portable dynamic signal test and analysis system was used for on-site dynamic testing. The data acquisition system was connected to a computer for real-time signal acquisition, storage, display, and analysis. The acquisition equipment is shown in Figure 4.

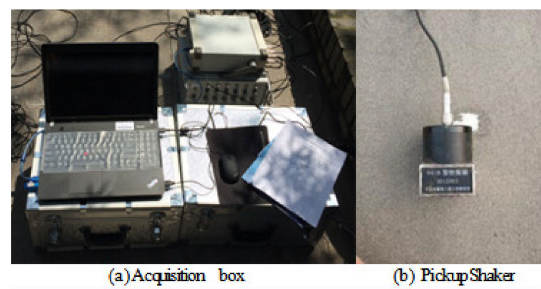


Figure 4. Acquisition equipment used for dynamic testing.

A total of six measurement points were selected, including three at the bottom of the arch (P1–P3) and three at the top of the arch (P4–P6). First, the Pickup Shaker was fixed to the plasticine, and then the plasticine was fixed at each measurement point. Two pickup shakers were placed at each measurement point, one for the horizontal (east–west) direction and the other for the vertical direction. The arrangement of the measurement points is shown in Figure 5.

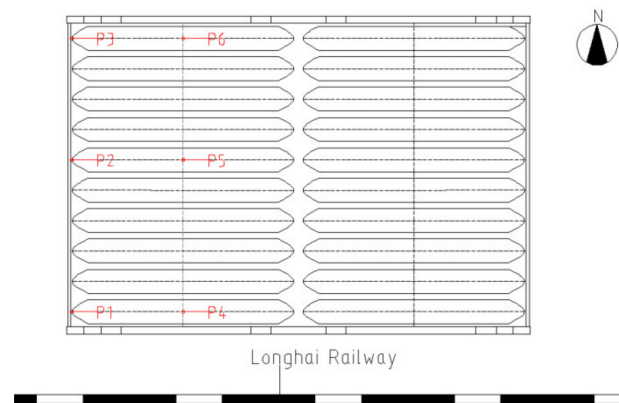


Figure 5. A graphical illustration showing the arrangement of the measurement points.

The first structural dynamic test, that is, the measurement of the dynamic characteristics of the thin-shell factory, was performed under the action of ground pulsations. The velocity and acceleration at each measurement point were acquired separately, and the acquisition time for each measurement was 10 min. The signals were pre-collected for at least 3 min before each acquisition to ensure the reliable connection of the test equipment. Velocity and acceleration were measured in the three groups, and no trains or pedestrians passed next to the test area during the test.

Subsequently, a train dynamic test, measuring the dynamic response of the thin-shell factory under the vibration load of a train was conducted, and the velocity and acceleration for each measurement point were acquired.

4. Test Results and Analysis

4.1. Results Pre-Processing

In the field of dynamic measurement, human influence as well as external factors can introduce bias, often resulting in the confusion of the collected vibration signal with the interference components. Therefore, before analyzing the acquired data, it was necessary to pre-process the data. Using DAS 2.0 software, the acquired data were pre-processed in four steps: removing abnormal signals, de-DC, digital filtering, and eliminating trend terms.

After the pre-processing was completed, the time and frequency domain waveforms of velocity and acceleration for each measurement point (P1–P6) were obtained. The waveforms under the action of ground pulsations of the velocity at P1, for example, are shown in Figures 6 and 7.

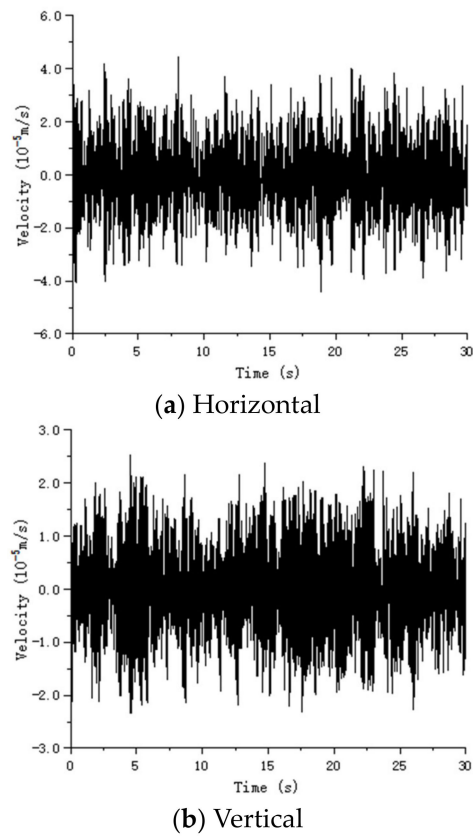


Figure 6. Time domain waveform of velocity at P1.

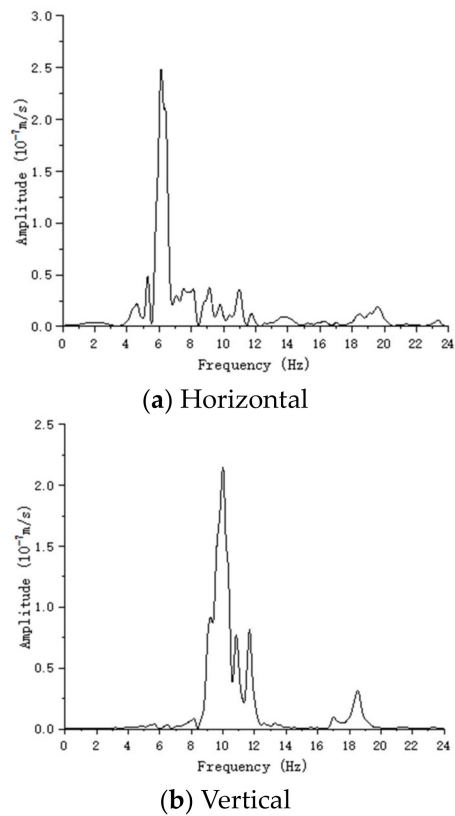


Figure 7. Frequency domain waveform of velocity at P1.

4.2. Dynamic Characteristic Analysis of the Thin-Shell Factory under the Action of Ground Pulsation

The dynamic test treated the factory as a multi-mass structure, and the factory was made to vibrate under natural excitation. Since natural pulsation is random, the vibration of the factory must also be random. Based on the random vibration theory, the ground pulsation can be regarded as a smooth random process, whereas the thin-shell factory can be regarded as a linear system, where both the damping and the self-oscillation frequency do not change with time; thus, the pulsation response of the factory is a smooth random process. For this process, the structure has the following relationship between the excitation and response [14]:

$$|H(\omega)|^2 = \frac{G_{yy}(\omega)}{G_{ff}(\omega)} \quad (1)$$

In the formula: $H(\omega)$ is the transfer function of the structure, ω is the circular frequency of the vibration, $G_{yy}(\omega)$ is the self-power spectrum of the structural reaction, and $G_{ff}(\omega)$ is the self-power spectrum of ground pulsation.

There can be several sources of noise present in the input signal while measuring dynamic characteristics, such as environmental vibrations, wind pulsations, and other vibration signals, which can obscure the acquisition of accurate input excitation signals. Thus, the input excitation signal can be approximated as finite-bandwidth white noise, meaning that $G_{ff}(\omega)$ is assumed to be a constant, so the performance of the reaction power spectrum of the structure can be reflected by the transfer function. If the frequency of the transfer function is close to its self-oscillation frequency, the transfer function will have a peak, and, according to this principle, the inherent frequency of the structure can be determined.

The above methods and principles were followed, and the frequencies corresponding to the velocity and acceleration were averaged to obtain the first-order and second-order inherent frequencies of the thin-shell factory [15], as shown in Table 1.

Table 1. Measured results of inherent frequency (Hz).

	First-Order Frequency	Second-Order Frequency
Horizontal	6.24	18.50
Vertical	9.31	19.28

4.3. Dynamic Response Analysis of the Thin-Shell Factory under Train Vibration Load

Figures 8 and 9 show the velocity and acceleration amplitude at each measurement point of the thin-shell factory under train excitation, and it can be seen:

1. With respect to velocity and acceleration, for all of the measurement points (P1–P6), the vertical amplitudes were larger than the horizontal amplitudes.
2. With respect to velocity and acceleration, for the three measurement points at the bottom of the arch, whether horizontal or vertical, the amplitude showed a decreasing trend ($P1 > P2 > P3$). Similarly, for the three points at the top of the arch, the amplitude also showed a decreasing trend ($P4 > P5 > P6$), indicating that the farther away from the railroad, the smaller the vibration.
3. When comparing the amplitude of velocity between the measurement points located at the same distance from the railroad, whether horizontal or vertical, the amplitude of the velocity was not significantly different between P1 and P4, P2 and P5, and P3 and P6, indicating that the velocity of the vibration at the bottom of the arch was basically the same as that at the top of the arch. When comparing the acceleration amplitudes of the measurement points located at the same distance from the railroad, whether horizontal or vertical, the acceleration amplitudes were as follows: $P1 > P4$, $P2 > P5$, and $P3 > P6$, indicating that the acceleration of the vibration at the bottom

of the arch was greater than that at the top of the arch, with an average amplitude of 40.64%.

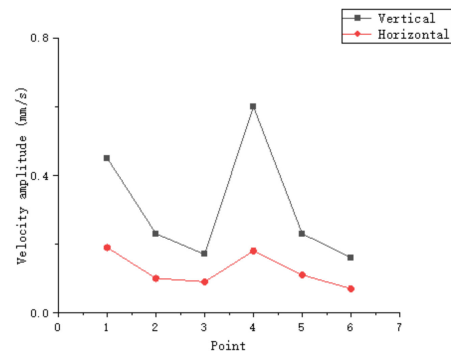


Figure 8. Velocity amplitude curve for each measurement point under train vibration load.

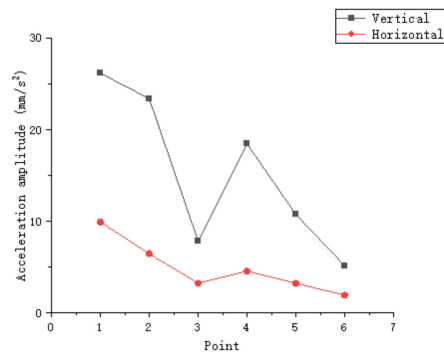


Figure 9. Acceleration amplitude curve for each measurement point under train vibration load.

5. Finite-Element Numerical Simulation Analysis

5.1. Establishment of the Finite-Element Model for the Thin-Shell Factory

The ABAQUS 6.14 finite-element software was used to generate a three-dimensional finite-element model of the thin-shell factory; shell cells were used based on the actual size and the characteristics of the structure, and the whole model was divided into 63,567 cells. The model is illustrated in Figure 10.

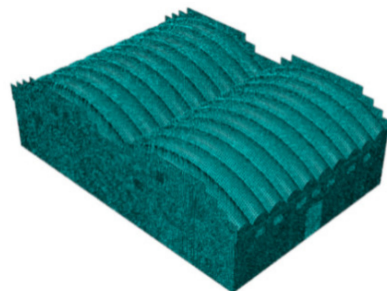


Figure 10. Finite-element model of the thin-shell factory.

The factory consists mainly of a concrete floor, brick walls, concrete beams, and brick arches. The physical parameters of each material, according to the current survey documents of the thin-shell factory and a review of the relevant codes [16], are listed in Table 2.

Table 2. Physical parameters of the materials used in the construction of the thin-shell factory.

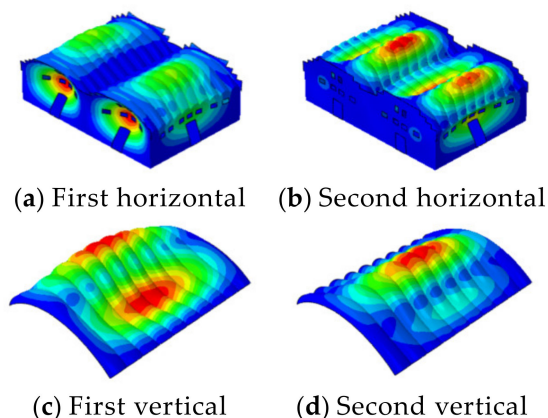
Material	Density (kg/m ³)	Elasticity Modulus (MPa)	Poisson's Ratio
Concrete	2400	20,000	0.167
Brick	1900	4500	0.15

5.2. Model Checking

The ABAQUS 6.14 software was used to solve the thin-shell factory structure, and the self-vibration frequency and vibration pattern of the structure were calculated by implementing the Lanczos algorithm. It was found that the vibration in the horizontal direction was the overall vibration of the factory, whereas the vibration in the vertical direction was the individual vibration of the double-curved brick arch. The simulation results were compared with the field dynamic characteristic test results, and the comparison and the first two orders of vibration patterns are shown in Table 3 and Figure 11, respectively.

Table 3. Comparison of measured and simulated frequencies of the thin-shell factory (Hz).

Oder	Direction	Simulation	Measurement	Error Rate (%)
First	Horizontal	6.72	6.24	7.14
	Vertical	9.86	9.31	5.58
Second	Horizontal	19.15	18.50	3.39
	Vertical	20.03	19.28	3.74

**Figure 11.** Simulation results of the first and second patterns of the thin-shell factory.

The results indicate that the self-oscillation frequencies obtained from the numerical simulation were greater compared with the field measurements. This might have been because the numerical simulation was carried out based on the assumption of complete elasticity. In contrast, the thin-shell factory, which is relatively old in construction, may have suffered from structural damage because of degradation of building-material properties, structural cracking, and other factors. Consequently, this could have led to degradation of structural stiffness, and the simulation results were greater than the results obtained from the measurements [17]. The maximum error rate was 7.14%, indicating that the errors of both measurements were within the acceptable range, and the reliability of the finite-element model was initially verified.

5.3. Establishment of the Finite-Element Model for the Soil Structure

The soil body was modeled using the solid cell approach and meshed using 17,395 C3D8 linear hexahedral cells. Chain-link constraints were used around and at the bottom of the soil body [18].

The contact relationship between the soil body and the factory structure can be defined as a tie constraint, so that the deformation between the two is common [19]. The overall model is shown in Figure 12.

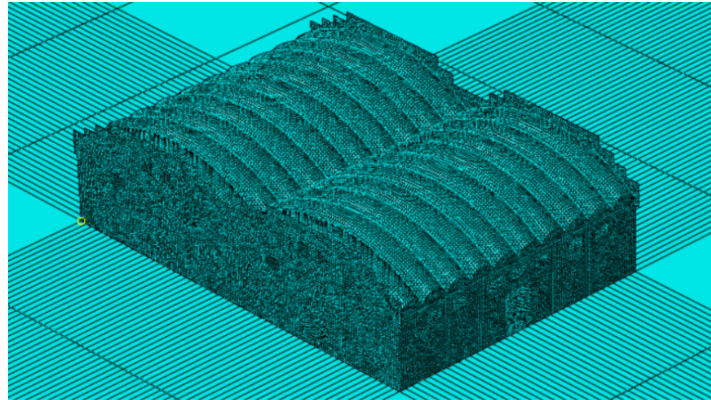


Figure 12. Overall finite-element model of soil structure.

Based on the literature [20] and the current survey documents of the thin-shell factory, the following mechanical parameters for the soil were used: elasticity modulus, $E = 29400$ kPa; density, $\rho = 1900$ kg/m³; and Poisson's ratio, $\mu = 0.25$.

Rayleigh damping [21,22] was used to obtain Rayleigh damping coefficients, α ($\alpha = 1.7506$) and β ($\beta = 0.0003866$).

5.4. Simulation of Train Vibration Load

Train load is transferred through the rail to the rail sleeper and then to the substructure; therefore, for a fixed wheelbase train, its effect on the substructure can be superimposed by a series of excitations.

The magnitude of the train vibration load is mainly determined by the vehicle's weight and wheels and the track structure. In this study, the excitation force function method [23–26] was used to calculate the train vibration load. In this method, the train vibration load is composed of the static load of the wheels, the vibration load caused by the wheels and other factors, the periodic vibration load generated by the wheel wear eccentricity on the track structure, and the forced vibration load of the train caused by untimely construction and track maintenance. The calculation formula for the train vibration load, $F(t)$, is as follows:

$$F(t) = P_0 + P_1 \sin \omega_1 t + P_2 \sin \omega_2 t + P_3 \sin \omega_3 t \quad (2)$$

In the formula: P_0 is the static wheel load; P_1 , P_2 , and P_3 are the train vibration load amplitudes under three control conditions, namely, smoothness of traffic, additional dynamic load applied on the line, and wear of the track waveform, respectively (Table 4); and ω_i is the circular frequency of the uneven wavelength corresponding to the train running speed, v , and can be expressed by the following formula:

$$\omega_i = 2\pi v / L_i \quad (i = 1, 2, 3) \quad (3)$$

where L_i is a typical wavelength corresponding to the three control conditions mentioned in Table 4 and t is the time.

Table 4. Geometric parameters for UK railway engineering.

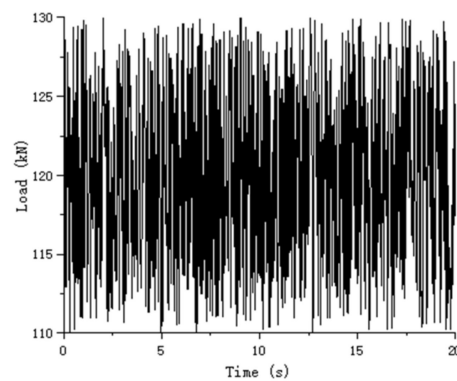
Condition of Control	L_i (m)	α_i (mm)
Smoothness of traffic ($i = 1$)	50.00	16.000
	20.00	9.000
	10.00	3.500
	5.00	2.500
Additional dynamic load applied to the line ($i = 2$)	2.00	0.400
	1.00	0.300
Wear of the track waveform ($i = 3$)	0.50	0.080
	0.05	0.005

If the under-spring mass of the train is M_0 , then its corresponding vibration load amplitude, P_i , is:

$$P_i = M_0 \alpha_i \omega_i^2 \quad (i = 1, 2, 3) \quad (4)$$

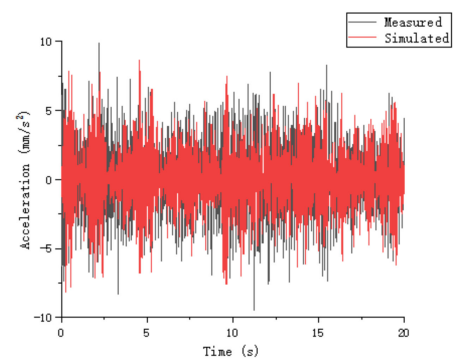
where α_i is the typical vector height corresponding to the three control conditions listed in Table 4.

Based on domestic and foreign railroad standards and field observations, the following values were assumed: the axle weight of the vehicle was set as 24 t, the under-spring mass as $M_0 = 1990$ kg, the unilateral static wheel weight of the train as $P_0 = 120$ kN, and the speed as 60 km/h. Then, based on the geometric unevenness management values presented in Table 4, the L and α values were set as follows: $L_1 = 10$ m, $\alpha_1 = 3.5$ mm; $L_2 = 2$ m, $\alpha_2 = 0.4$ mm; and $L_3 = 0.5$ m, $\alpha_3 = 0.08$ mm. The load time curve of the train was plotted in Origin 2021 software, and the load was shown to vibrate in the range of 110–130 kN, as shown in Figure 13.

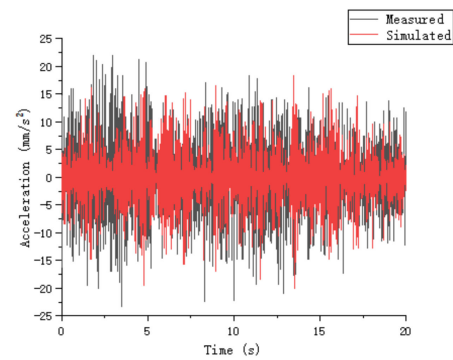
**Figure 13.** Time history curve of the train vibration load.

5.5. Dynamic Response Checking

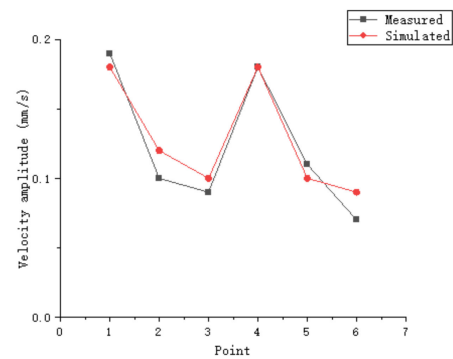
The train vibration load simulated by the excitation force function method was entered at the corresponding position in the model. Then, the acceleration response curves for each measurement point were extracted, the amplitude values were obtained and compared with the corresponding field measured data [27], and the two matched well, as shown in Figure 14 (for the limitation of space, only the acceleration curve of P2 is listed) and Figures 15 and 16.



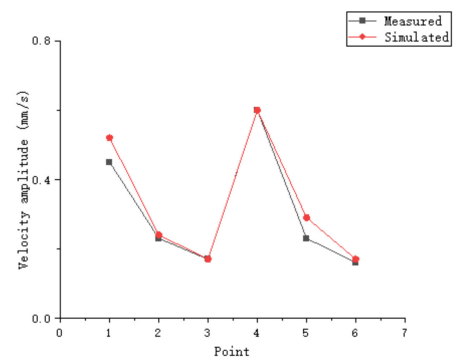
(a) Horizontal



(b) Vertical

Figure 14. Comparison of simulated and measured acceleration time domain waveforms at P2.

(a) Horizontal



(b) Vertical

Figure 15. Comparison of simulated and measured velocity amplitude curves for each measurement point.

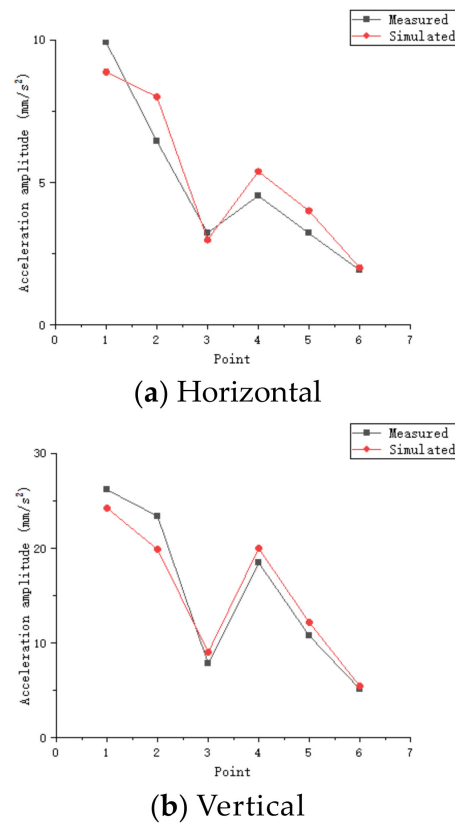


Figure 16. Comparison of simulated and measured acceleration amplitude curves for each measurement point.

In summary, the calculation results of the model can quantitatively reflect the actual vibration response for each measurement point when a train passes through the thin-shell factory, which further verifies the reliability of the finite-element model.

5.6. Analysis of the Dynamic Response of the Thin-Shell Factory under Different Train Vibration Loads

On the basis of the calculations in this paper, by changing the running speed of the train to study the effect of vibration load on the dynamic response of the thin-shell factory under different train running speeds and taking train running speeds of 80 km/h, 100 km/h, 120 km/h, 150 km/h, and 250 km/h (high-speed rail) as five cases to study, the thin-shell factory acceleration and velocity amplitude change law for each measurement point were determined, as shown in Figure 17 (where the horizontal direction indicates the east–west direction).

From Figure 17, it can be seen that the vertical acceleration amplitude, vertical velocity amplitude, horizontal acceleration amplitude, and horizontal velocity amplitude were all positively correlated with train running speed. For every 20 km/h increase in train running speed, the average increase in the vertical acceleration amplitude, vertical velocity amplitude, horizontal acceleration amplitude, and horizontal velocity amplitude for each measurement point of the thin-shell factory was 35.4%, 29.8%, 23.7%, and 12.5%, respectively. It can be seen that the increase in train running speed has the greatest effect on the amplification of vertical acceleration amplitude and the least effect on the amplification of horizontal velocity amplitude.

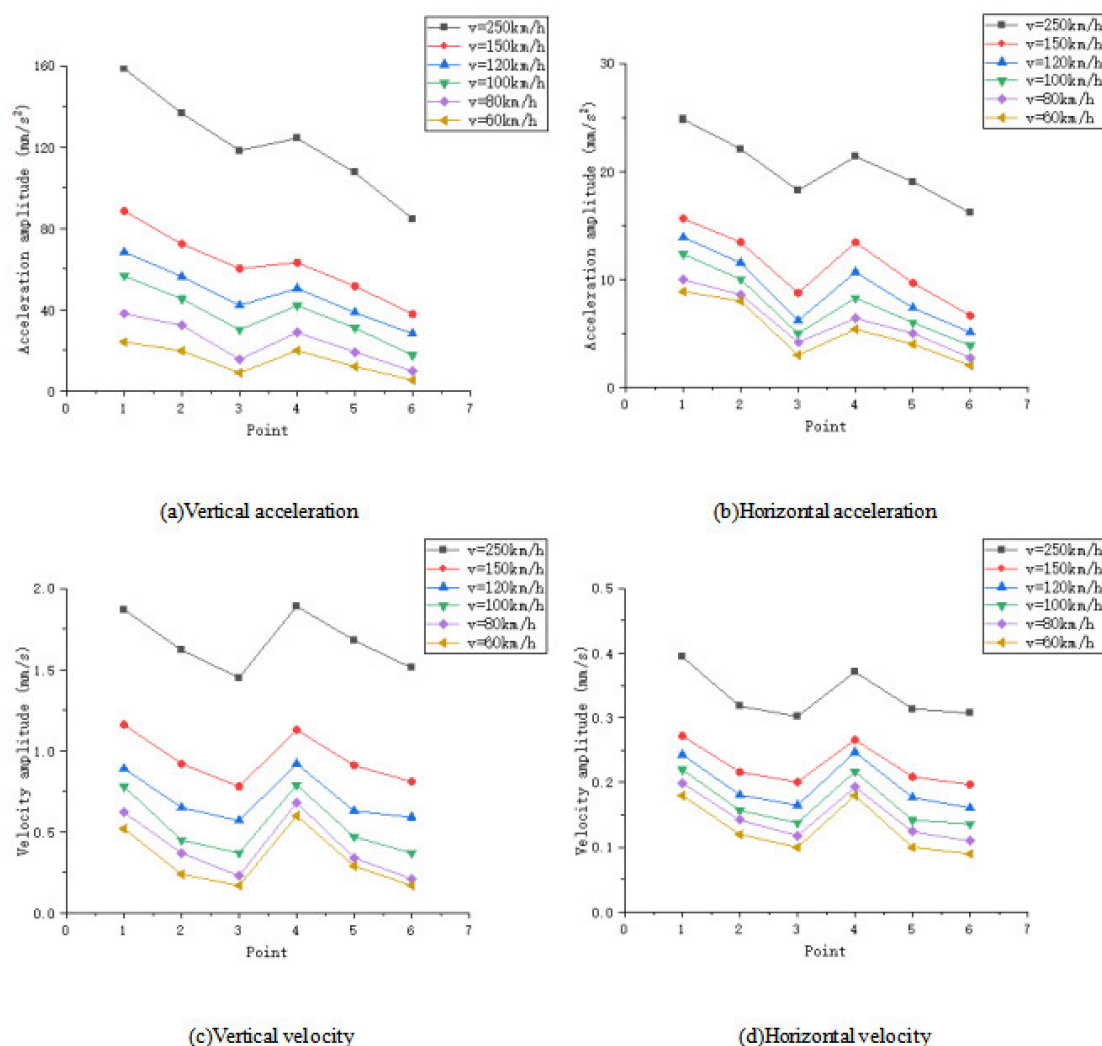


Figure 17. Vibration amplitude curves for each measurement point under different train running speeds.

6. Vibration Evaluation of the Thin-Shell Factory

Both domestic and foreign building structure allowable vibration standards are based on the peak particle velocity (PPV) as the vibration limit value for ancient building control. The statistics for some of the vibration standards relevant to this paper are shown in Table 5. Integrity in Table 5 relates to whether a building is damaged, with building damage usually referring to the fatigue of non-load-bearing elements of ancient buildings under the action of micro-vibrations due to cumulative damage resulting from surface cracking, spalling, and other phenomena, while security relates to whether a structure is damaged, which usually refers to the strong vibration of ancient buildings under the action of load-bearing elements of damage that endanger the safety of the structure.

As can be seen from Table 5, most of the vibration standards for building structures at home and abroad are proposed for the security of the structure, and the lower limit of PPV is mainly between 1.8 and 12.7 mm/s, which means that when the vibration is less than this lower limit, it usually does not cause structural damage.

Table 5. Summary of domestic and foreign ancient building control standards.

Standards/Scholars	Vibration Amplitude Limit (mm/s)	Frequency Range (Hz)	Control Standards	Note Description
International Standard ISO 2631 [28]	2.5~10	--	Security	
German Standard DIN 4150-3 [29]	2.5	1~10	Security	Structures affected by continuous long-term vibration; horizontal velocity limit for the top floor of a structure
Swiss Standard SN 640312a [30]	3.0	10~30	Security	Vibration source for machinery, transportation, and construction equipment
Federal Transit Administration FTA Standard [31]	3.08	--	Security	
Anti-Industrial Vibration of Ancient Buildings Technical Specification (GB/T50452-2008) [32]	0.15~0.2	--	Integrity	National key cultural relics protection unit of ancient masonry load-bearing structures at the highest water-level velocity limit
Remington [33]	2	--	Security	
Konon, Schuring [34]	6.4~12.7	10~40	Security	
YANG Xianjian, PAN Fulan [35]	1.8	--	Security	

The “Anti-industrial Vibration of Ancient Buildings Technical specification” (GB/T 50452-2008) was proposed for the integrity of buildings. Its development was based on the long-lasting effects of vibration, while taking into account the security and integrity of buildings, and was proposed as a fatigue limit as the basis for vibration standards, so that its requirements regarding micro-vibrations are currently the most stringent among similar standards in the international arena. The specification specifies allowable vibration values in accordance with the type of ancient building structure, the materials used, the level of protection, and the propagation speed of elastic waves in the ancient building structure. For the national heritage protection units of ancient masonry structure, the vibration limit is between 0.15 and 0.2 mm/s. The security and integrity of old industrial buildings are much better compared to ancient buildings, and their limits can be allowed to be increased appropriately. Thus, for this factory, it was assumed that its security limit is 2.5 mm/s and that its integrity limit is 0.27 mm/s.

The velocity amplitude for each measurement point of the thin-shell factory under different train running speeds was extracted, as shown in Tables 6 and 7, and compared with the limit values in Table 5. It is clear that when $v = 150$ km/h, the maximum velocity amplitude is 1.163 mm/s, which is less than the vibration control lower limit of 2.5 mm/s for the security of the thin-shell factory, such that the security of the thin-shell factory meets the requirement, and the maximum horizontal velocity amplitude is 0.272 mm/s, which just exceeds the lower limit of 0.27 mm/s for the integrity of the thin-shell factory, such that the integrity of the thin-shell factory just exceeds the requirement. When $v = 250$ km/h, the maximum horizontal velocity amplitude is 0.394 mm/s, which exceeds the corresponding normative limit, indicating that the integrity of the thin-shell factory does not meet the requirement completely. Therefore, it is recommended to the transportation department

that the train should not run at a speed of more than 150 km/h and that the thin-shell factory strengthen the monitoring and protection of its integrity.

Table 6. Vertical velocity amplitude for each measuring point under different train running speeds (mm/s).

	V = 60 km/h	V = 80 km/h	V = 100 km/h	V = 120 km/h	V = 150 km/h	V = 250 km/h
P1	0.522	0.625	0.786	0.891	1.163	1.871
P2	0.246	0.374	0.451	0.659	0.927	1.623
P3	0.178	0.235	0.377	0.578	0.780	1.454
P4	0.605	0.689	0.794	0.921	1.132	1.896
P5	0.293	0.342	0.478	0.632	0.918	1.685
P6	0.174	0.214	0.376	0.598	0.811	1.518

Table 7. Horizontal velocity amplitude for each measuring point under different train running speeds (mm/s).

	V = 60 km/h	V = 80 km/h	V = 100 km/h	V = 120 km/h	V = 150 km/h	V = 250 km/h
P1	0.182	0.199	0.220	0.243	0.272	0.394
P2	0.126	0.142	0.157	0.181	0.216	0.318
P3	0.103	0.118	0.138	0.165	0.201	0.302
P4	0.184	0.193	0.217	0.247	0.266	0.371
P5	0.107	0.124	0.142	0.177	0.209	0.314
P6	0.098	0.110	0.136	0.161	0.197	0.307

7. Conclusions

Through field dynamic tests and finite-element numerical simulations, the dynamic characteristics of a thin-shell factory with a multi-span double-curved brick arch in Changleyuan in Baoji City were analyzed, the influence of train vibration load on the dynamic response of the thin-shell factory was investigated, and a vibration evaluation of the thin-shell factory was carried out. The following main conclusions were derived:

- (1) The field dynamic test results of the thin-shell factory show that the first- and second-order frequencies in the horizontal direction of the structure were 6.24 Hz and 18.50 Hz, respectively, and that the first- and second-order frequencies in the vertical direction were 9.31 Hz and 19.28 Hz, respectively.
- (2) The vibration in the horizontal direction is the overall vibration of the factory, whereas the vibration in the vertical direction is the individual vibration of the double-curved brick arch.
- (3) The self-oscillation frequency obtained from the numerical simulation results (which were based on the assumption of complete elasticity) was greater compared with the field measurements because of the reduced structural stiffness. Additionally, the maximum error rate was only 7.14%.
- (4) Both in acceleration and velocity, the vertical vibration for each measurement point was larger than the horizontal vibration, and the farther away from the railroad, the smaller the vibration. The velocity of the vibration at the bottom of the arch was almost the same as that at the top of the arch, while the acceleration of the vibration at the bottom of the arch was significantly larger than that at the top of the arch, with an average amplitude of 40.64%.
- (5) For every 20 km/h increase in train running speed, the average increase in the vertical acceleration amplitude, vertical velocity amplitude, horizontal acceleration amplitude, and horizontal velocity amplitude for each measurement point of the thin-shell factory was 35.4%, 29.8%, 23.7%, and 12.5%, respectively.

- (6) When $v = 150$ km/h, the maximum velocity amplitude for each measurement point of the thin-shell factory was 1.163 mm/s, which is less than the security specification limit of 2.5 mm/s, such that the security of the thin-shell factory meets the requirement, and the maximum horizontal velocity amplitude was 0.272 mm/s, which is close to the integrity specification limit of 0.27 mm/s, such that the integrity of the thin-shell factory just exceeds the requirement; so it is suggested that train running speeds should not exceed 150 km/h and that the thin-shell factory needs to strengthen the monitoring and protection of its integrity.

Author Contributions: Conceptualization, Y.Z.; Methodology, P.M.; Software, Y.W.; Formal analysis, M.Z.; Investigation, J.J.; Data curation, X.N.; Writing—original draft, Y.L.; Writing—review & editing, J.S. All authors have read and agreed to the published version of the manuscript.

Funding: This research was funded by 2022 Shaanxi Province Construction Science and Technology Plan Project grant number 2022-S32 and The APC was funded by Xi'an University of Technology.

Data Availability Statement: I hereby declare that the data I use in this article can not be provided or obtained due to privacy concerns.

Conflicts of Interest: The authors declare no conflict of interest.

References

- Zhang, Y. *Influence of Urban Rail Transit Vibration on Ancient Buildings*; Soochow University: Suzhou, China, 2016.
- Xia, Q.; Mao, N.; Wang, D.; Gao, H.; Zhao, J. Research and evaluation of vibration responses of ancient pagoda of Liao Dynasty under different train excitation. *Noise Vib. Control* **2020**, *40*, 199–205.
- Qiao, X.; Liu, W.; Luo, W.; Ni, W.; Yang, X.; Huang, J.; Liu, J. Field measurement and numerical analysis of influence of traffic load on vibration of Shuangjingzibao ancient city wall. *J. Vib. Eng.* **2023**, *36*, 1–13.
- Zhang, S.; Tian, P.; Zhang, F.; Lu, J.; Yuna, Z.; Mao, D. Analysis of the dynamic response for Xi'an Drum-Tower under the vibration of urban rail transit. *J. Basic Sci. Eng.* **2021**, *29*, 1292–1307.
- Tian, T.; Lei, Y.; Qi, F. Vibration response transmission of lining arch due to train speed-changing vibration load. *Eng. Mech.* **2018**, *35*, 143–151.
- Karpenko, M.; Skačkauskas, P.; Prentkovskis, O. Methodology for the Composite Tire Numerical Simulation Based on the Frequency Response Analysis. *Ekspluat. I Niezawodn. Maint. Reliab.* **2023**, *25*, 1–11. [[CrossRef](#)]
- Sanayei, M.; Maurya, P.; Moore, J.A. Measurement of building foundation and ground-borne vibrations due to surface trains and subways. *Eng. Struct.* **2013**, *53*, 102–111. [[CrossRef](#)]
- Hinzen, K.G. Subway-induced vibrations in cologne cathedral. *Seismol. Res. Lett.* **2014**, *85*, 631–638. [[CrossRef](#)]
- Javad Sadeghi, M. Hassan Esmaili. Safe distance of cultural and historical buildings from subway lines. *Soil Dyn. Earthq. Eng.* **2017**, *96*, 89–103.
- Agostinacchio, M.; Ciampa, D.; Diomedì, M.; Olita, S. Parametrical analysis of the railways dynamic response at high speed moving loads. *J. Mod. Transp.* **2013**, *21*, 169–181. [[CrossRef](#)]
- Ju, S.-H.; Lin, H.-T. Experimentally investigating finite element accuracy for ground vibrations induced by high-speed trains, Engineering Structures. *Eng. Struct.* **2008**, *30*, 733–746. [[CrossRef](#)]
- Stosiak, M.; Karpenko, M.; Prentkovskis, O.; Deptuła, A.; Skačkauskas, P. Research of vibrations effect on hydraulic valves in military vehicles. *Def. Technol.* **2023**, *in press*. [[CrossRef](#)]
- Du, S. Changleyuan: Exploring the “Industrial Wonders of China’s War Effort”. *New West* **2021**, *10*, 5–10.
- Liu, J.; Du, X. *Structural Dynamics*; Machinery Industry Press: Beijing, China, 2005.
- Wang, D. *The Test Dynamic Characteristics and Analysis of Lafonce Office Building in Xi'an*; Xi'an University of Technology: Xi'an, China, 2018.
- GB 50003-2011; Masonry Structure Design Code. Ministry of Housing and Urban-Rural Development: Beijing, China, 2011.
- Lu, J.; Si, J.; Tian, P.; Zhang, W. Dynamic characteristic test analysis of Jishi Pagoda of Xingjiao Temple. *Build. Struct.* **2017**, *47*, 105–108.
- Liu, J.; Huan, Y.; Li, J. Application of artificial boundary and seismic input in general finite element software. *Chin. J. Undergr. Space Eng.* **2011**, *7*, 1774–1779.
- Wang, T.; Ding, J.; Lou, M.; Yu, J. Subway-induced building vibration and its propagation. *China Civ. Eng. J.* **2009**, *42*, 33–39.
- Wang, W.; Guo, X. Stability and characteristics of landscape in Changleyuan area at the north side of the Weihe river in Baoji. *Geol. Shaanxi* **2021**, *39*, 75–83.
- Hu, B.; Wang, Y.; Ling, D. Physical essence and influence of model parameters on dynamic response of Rayleigh damping. *J. Zhejiang Univ. (Eng. Sci.)* **2017**, *51*, 1284–1290.

22. Li, L.; Zhang, B.; Yang, X. Analysis of dynamic response of large cross-section tunnel under vibrating load induced by high speed train. *Chin. J. Rock Mech. Eng.* **2005**, *24*, 4259–4265.
23. Mo, H.; Deng, F.; Wang, J. Analysis of dynamic response of shield tunnel during metro operation. *Chin. J. Rock Mech. Eng.* **2006**, *25*, 3507–3512.
24. Liang, B.; Cai, Y. Dynamic analysis on subgrade of high speed railways in geometric irregular condition. *J. China Railw. Soc.* **1999**, *21*, 93–97.
25. Hu, Z.; Li, J. Subway train load analysis methods. *Subgrade Eng.* **2006**, *15*, 18–20.
26. Ding, Z.; Xie, H.; Peng, L. Dynamic Response properties of soft bedrock of high speed railway tunnel. *J. Kunming Univ. Sci. Technol. (Nat. Sci.)* **2013**, *38*, 36–41+79.
27. Tian, T.; Li, G.; Qi, F.; Dong, J. Analysis on acceleration response of tunnel lining under vibration load of train with speed of 300 km/h. *J. China Railw. Soc.* **2020**, *42*, 112–120.
28. *ISO 2631; Mechanical Vibration and Shock-Evaluation of Human Exposure to Whole Body Vibration*. International Organization for Standardization (ISO): Zürich, Switzerland, 1989.
29. *DIN 4150-3; Structural Vibration Part 3: Effects of Vibration on Structure*. German Institute for Standards: Berlin, Germany, 1999.
30. *SN 640312A; Effects of Vibration on Construction*. Schweizerische Normenvereinigung SNV: Zürich, Switzerland, 1992.
31. *FTA-VA-90-91003-06; Transit Noise and Vibration Impact Assessment*. Federal Transit Administration: Washington, DC, USA, 2006.
32. *GB/T 50452-2008; Anti-Industrial Vibration of Ancient Buildings Technical Specification*. China Construction Industry Press: Beijing, China, 2008.
33. Remington, P.J.; Kurzweil, L.G. *Low—Frequency Noise and Vibrations from Trains*; Butterworth & Co., Ltd.: London, UK, 1987.
34. Konon, W.; Schuring, J.R. Vibration criteria for historic buildings. *J. Constr. Eng. Manag.* **1985**, *111*, 209–215. [[CrossRef](#)]
35. Yang, X.; Pan, F. Vibration protection of ancient buildings in environmental vibration. In *Proceedings of the Seventh Academic Conference on Geomechanics and Foundation Engineering of the Chinese Civil Engineering Society*; China Construction Industry Press: Beijing, China, 1994; pp. 674–678.

Disclaimer/Publisher’s Note: The statements, opinions and data contained in all publications are solely those of the individual author(s) and contributor(s) and not of MDPI and/or the editor(s). MDPI and/or the editor(s) disclaim responsibility for any injury to people or property resulting from any ideas, methods, instructions or products referred to in the content.